8. GRAIN-SIZE RECORD OF OCEAN CURRENT WINNOWING IN OLIGOCENE TO PLEISTOCENE OOZE, BROKEN RIDGE, SOUTHEASTERN INDIAN OCEAN[1]

Martha A. House,[2] David K. Rea,[2] and Thomas R. Janecek[3]

ABSTRACT

At Ocean Drilling Program Sites 752 and 754, located on Broken Ridge in the eastern Indian Ocean, we recovered a sequence of shallow-water pelagic sediments that span the past 90 m.y. The Oligocene to Pleistocene portion of these sediments are unconsolidated carbonate oozes that display a coherent variation in bulk grain size. We believe these sediments to be winnowed, and suggest that their grain size is a measure of that winnowing energy. The largest increase in grain size, interpreted to represent an enhancement in the energy of ocean currents, occurs in the earliest late Miocene. This increase occurs about 20 m upcore from the oxygen isotope indication of ice-volume increase about 13 Ma, and is about 3 m.y. younger. If this distinct temporal separation between proxy indicators of ice volume and of current intensity observed in the Broken Ridge cores is correct, the general impression of paleoclimatologists that the planetary temperature gradient and therefore atmospheric and oceanic circulation intensity varies directly with ice volume needs to be reconsidered.

INTRODUCTION

The $\delta^{18}O$ record of paleoclimate contains an ice-volume and a temperature component because both increasing ice volume and decreasing temperature (also increasing salinity) result in more positive $\delta^{18}O$ values in calcite formed in seawater. It is important to be able to separate these two phenomena for a number of reasons. That which we wish to address here is the effect of polar cooling on atmospheric and oceanic circulation. Atmospheric circulation responds directly to the pole-to-equator temperature gradient; steeper gradients incur stronger zonal winds. Inasmuch as the sea-surface circulation is wind-driven, the ocean surface circulation responds similarly to changes in the pole-to-equator temperature gradient. The serendipitous discovery of winnowed sediment on Broken Ridge allows us to bring an important new data set to bear on the question of when, during the course of the Tertiary global cooling, the ocean responded with increased vigor of sea-surface circulation.

The $\delta^{18}O$ shift toward positive values in the middle Miocene has been interpreted to reflect the growth of significant amounts of ice on Antarctica (Savin et al., 1975; Miller et al., 1987). Savin et al. (1975) suggested that this event coincided with a sudden cooling at high latitudes, with only minimal temperature change in the low latitudes (perhaps even a slight warming), and, therefore, with an important increase in the planetary (latitudinal) temperature gradient. Kennett (1977), discussing the same phenomena, attributed the growth in Antarctic ice volume to an increase in moisture supply and noted that important cooling may not have begun until the end of the middle Miocene. Matthews and Poore (1980) postulated that the middle Miocene $\delta^{18}O$ shift was entirely the result of bottom-water cooling with minimal associated ice growth. Woodruff et al. (1981) explicitly stated the assumption that the middle Miocene ice growth event was coincidental with an increase in the pole-to-equator temperature gradient. Kennett (1985) discussed the middle Miocene $\delta^{18}O$ shift in the Deep Sea Drilling Project (DSDP) Leg 90 cores east of Australia and remarked on indications of a younger cooling episode that occurs about 3 m.y. after the isotopic shift.

To examine questions of the timing of changes in the planetary temperature gradient and consequent changes in atmospheric and sea-surface circulation, and to avoid the ambiguities of the ice volume and/or temperature effects on the $\delta^{18}O$ record (e.g., Matthews and Poore, 1980), paleoceanographers must turn directly to proxy records of atmospheric and ocean surface circulation. Rea and Bloomstine (1986) and Rea (1989), reporting on the eolian dust proxy record of Southern Hemisphere atmospheric circulation, found that the intensity of the zonal winds increased at the end of the middle Miocene, about 3 m.y. younger than the time of the oxygen isotope shift. This information is consistent with the suggestion that the ice growth event did not involve a significant increase in the pole-to-equator temperature gradient that drives the atmospheric circulation. Information on the variations in the intensity of ocean surface circulation has been somewhat harder to ascertain. Perhaps the best such record has been the opal sedimentation history of the equatorial Pacific provided by Leinen (1979). She showed that opal fluxes began to increase about 15 Ma and reached a maximum about 8 to 10 Ma, and suggested that this event recorded the intensification of the Southern Hemisphere trade winds that drive the equatorial upwelling. Miller et al. (1987) noted that 10 Ma may have been a time of enhanced erosion along the Atlantic continental margin of North America and that 14 Ma was not, although data from that latter interval are sparse.

OPPORTUNITY AT BROKEN RIDGE

The plateau region of Broken Ridge lies at a depth of 1000 to 1100 m (Fig. 1) and is underlain by a foraminifer or foraminifer-bearing nannofossil ooze. This ooze reaches a maximum thickness of about 120 m at Site 754 near the center of the platform and thins to the north and south. A layer of sand and limestone pebbles denotes a lower Oligocene disconformity and divides the ooze into upper and lower portions. The upper ooze unit, from which most of our samples are derived, ranges in age from Pleistocene to middle Oligocene. The ooze below the Oligocene disconformity, of late Eocene age, was poorly recovered and we
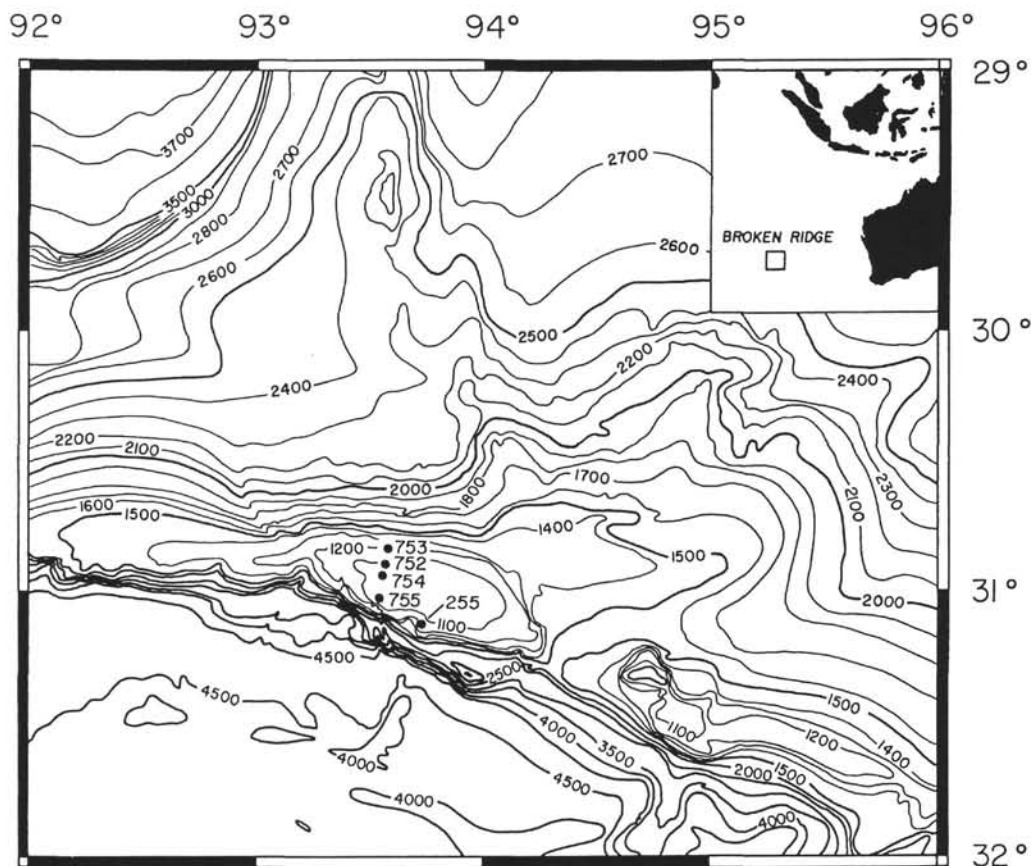
Figure 1. Location of ODP/DSDP drill sites on Broken Ridge, eastern Indian Ocean.

have only a few samples from that interval (Peirce, Weissel, et al., 1989).

The pelagic ooze atop Broken Ridge was deposited in water depths ranging from sea level at the time of the mid-Oligocene disconformity to the present depths of about 1100 m (Rea et al., 1990). At present this depth lies near the bottom of the main thermocline and thus near the boundary between the surface and Antarctic Intermediate Water masses; given any reasonable subsidence history for Broken Ridge, these pelagic oozes should reflect the hydrology and chemistry of the surface water layer for essentially all of their depositional history.

The shipboard scientific party of DSDP Leg 26, which drilled about 20 km away from the Ocean Drilling Program (ODP) Leg 121 transect at Site 255 (Fig. 1), interpreted these Oligocene to Pleistocene oozes as winnowed (Davies, Luyendyk, et al., 1974). The oozes recovered during Leg 121 were characterized by low sedimentation rates averaging about 0.3 to 0.6 cm/1000 yr, and rather high abundances of foraminifers (Peirce, Weissel, et al., 1989). The Leg 121 shipboard scientific party conducted a somewhat rudimentary grain-size analyses of the sediments from Sites 752 and 754, which are about 5.5 km apart, to test the concept of winnowing, and found indications of intercore regularity in the grain-size records (Rea et al., 1990). On the basis of these preliminary indications we suggest that the sediments capping Broken Ridge were winnowed by the ocean currents of the southern subtropical gyre as they swept over the ridge top, and that the resultant grain-size record of these bulk sediments is therefore a proxy for the circulation energy of that gyre, a paleocurrent meter.

The size of terrigenous grains extracted from sediments is often used to interpret the transport energy at the seafloor (Ledbetter and Johnson, 1976; Ledbetter, 1981, 1986), in lakes (Half-

man and Johnson, 1984), and in the atmosphere (Rea et al., 1985). In the ocean, winnowing by tidal and unidirectional currents is a common aspect of sedimentation shallower that perhaps 2500 m; slumping and other kinds of sediment redistribution may occur at any depth. Winnowing and reworking phenomena have been described for pelagic sediments on the basis of bulk or total sediment parameters in the Caribbean Sea (Prell, 1977), on the Walvis Ridge (Shackleton et al., 1984), in the South Pacific (Rea and Janecek, 1986), and from Broken Ridge in the Indian Ocean (Davies, Luyendyk, et al., 1974). The most extensive study of the processes and results of winnowing and reworking of carbonate pelagic sediments was conducted nearly 20 years ago under the auspices of the Panama Basin Project (van Andel, 1973). In the eastern equatorial Pacific, carbonate sediments on the Carnegie, Cocos, and Coiba ridges are winnowed, leaving coarse deposits of foraminifer sand atop the ridges and moving the finer nannofossil component downslope. In the Panama Basin, characterized by moderate to high biological productivity and a shallow calcite compensation depth (CCD) of about 3400 m, mechanical processes dominate the sediment distribution above 1500 to 2000 m with dissolution becoming important below that depth (Moore et al., 1973; Kowsmam, 1973; van Andel, 1973; Dowding, 1977). The same processes occur on Walvis Ridge in the Southeast Atlantic (and at the same latitude as Broken Ridge) where productivity is lower than in the Panama Basin and the CCD is deeper, in excess of 4600 m (van Andel et al., 1977). There, the shallower ridge crest sites at 1054 m and 2467 m are winnowed with the finer carbonate fraction showing higher accumulation rates farther down the ridge flank (Shackleton et al., 1984; Moore et al., 1984). We expect these same processes to occur at shallow to intermediate depths in the eastern Indian Ocean where the fo-

raminiferal lysocline occurs at 3800 m (Peterson and Prell, 1985) and the CCD is rather deep, at about 5200 m (van Andel, 1975).

It is the intent of this paper to determine the winnowing size record for the southeastern Indian Ocean in detail and compare it to the $\delta^{18}O$ record derived from benthic foraminifers picked from the same samples to provide a cogent test for the suggestion of Kennett (1977, 1985) that the Miocene increase in the planetary temperature gradient and associated increase in circulation energies may have occurred a few million years after the increase in Antarctic ice volume.

METHODS AND STRATIGRAPHY

Continuous cores recovered with the advanced hydraulic piston corer from Holes 752A and 754A were sampled at regular intervals, commonly one sample per section, to provide the data for this study (Tables 1 and 2). Samples entering the laboratory were freeze-dried prior to analysis. Following freeze-drying, the samples were split, half to be screen sieved, and half to be processed for grain-size distribution on a Coulter Multisizer. The dried samples were then sieved in a stack of 63-μm, 150-μm, and 425-μm screens. Each sieve-size fraction was dried and weighed, allowing calculation of the weight percent of each size component. Benthic foraminifers for the isotopic analyses were picked from the larger size fractions (see Rea et al., this volume).

For processing on the Coulter Multisizer a portion of each bulk sample was mixed with an electrolyte solution, Isoton-II. Subsamples were sieved through a 50-μm screen, thus separating them into fine and coarse fractions. This sieve size was chosen because each Multisizer counting tube has a range of sensitivity from 2%–75% of the diameter of the tube orifice. The finer portions were run on the Multisizer with a 100-μm orifice, thus accounting for particle sizes ranging down to 2 μm. The coarse fraction suspensions were then processed with a 560-μm tube orifice, corresponding to a measured grain size of 12 μm to 420 μm. Each sample was run twice and resulting values averaged. From this, Coulter Multisizer software was used to generate overlaps of data from both tube sizes for each sample average. From this, the Multisizer software computed the median grain size for each core, as well as grain-size data corresponding to pre-selected percentiles (Tables 1 and 2).

In this discussion we will refer to the nannofossil stratigraphy as determined aboard the *JOIDES Resolution* and reported by Peirce, Weissel, et al. (1989). The zonations were referred to the mid-latitude biostratigraphic scheme of Bolli et al., (1985), which is slightly different than the time scale of Berggren et al. (1985), especially in the Miocene. For instance the lower/middle Miocene boundary in the Bolli et al. (1985) time scale is at the Zone CN4/CN5 boundary, 15.4 Ma; the same boundary in the Berggren et al. (1985) time scale is between nannofossil Zones CN3 and CN4, at 16.5 Ma. Persons interested in the details of the biostratigraphy should consult Peirce, Weissel, et al. (1989) and Pospichal et al. (this volume). Additional information on nannofossil zonations in the Miocene was provided by P. Resiwati (pers. comm., 1990).

GRAIN SIZE AND $\delta^{18}O$ RECORDS FROM BROKEN RIDGE

Weight-percent data resulting from sieving show similar results for both sites. For both cores, the total amount of material coarser than 63 μm is chosen to illustrate changes in depositional environment. The median grain size as plotted in micrometers supplies similar and equally informative data (Figs. 2 and 3). Ensuing discussions refer to the percent coarse material plots.

The pelagic oozes of Holes 752A and 754A exhibit similar grain-size patterns (Figs. 2 and 3). Both records show a Pleistocene peak above 80% coarser than 63 μm, an interval of relatively

coarse grains continuing down through most of the upper Miocene, a marked decline in grain size to low values of about 30% to 40% coarser than 63 μm which pertain through much of the middle Miocene, and slightly coarser material above a minimum in the lower Miocene at 80.75 meters below seafloor (mbsf) in Hole 752A and 95.18 mbsf in Hole 754A. Sediment grain size

Table 1. Gain-size data from Hole 752A.

Core, section, interval (cm)	Depth (mbsf)	Material on μm screen			Total coarse fraction (%)	Median grain size (μm)
		63 μm (wt%)	150 μm (wt%)	425 μm (wt%)		
121-752A-						
1H-1, 80–82	0.80	26.57	55.32	1.47	83.36	145.70
1H-2, 80–82	2.30	33.25	39.32	2.33	74.89	133.40
1H-3, 80–82	3.80	34.28	29.81	1.86	65.95	119.60
1H-4, 80–82	5.30	35.98	29.69	1.39	67.05	117.00
1H-5, 80–82	6.80	23.29	28.60	4.77	56.66	69.68
2H-1, 80–82	9.10	23.76	31.13	2.63	57.52	104.20
2H-2, 80–82	10.60	26.94	34.48	2.32	63.73	120.80
2H-3, 80–82	12.10	25.16	34.48	3.83	63.47	83.62
2H-4, 80–82	13.60	23.31	34.99	1.67	59.97	148.60
2H-5, 80–82	15.10	27.96	33.48	2.52	63.95	67.67
2H-6, 80–82	16.60	22.96	24.63	2.48	50.08	61.55
3H-1, 80–82	18.60	34.10	23.02	1.23	58.35	73.36
3H-2, 78–80	20.08	34.42	29.96	1.52	65.90	65.17
3H-3, 80–82	21.60	31.04	31.63	1.12	63.79	66.65
3H-4, 78–80	23.08	47.18	24.83	0.73	72.73	54.68
3H-5, 80–82	24.60	27.05	25.36	1.19	53.60	58.21
3H-6, 80–82	26.10	30.35	21.67	0.79	52.80	87.78
4H-1, 80–82	28.10	34.19	36.12	0.64	70.96	125.90
4H-2, 80–82	29.60	30.28	31.97	1.48	63.73	73.08
4H-3, 80–82	31.10	30.26	33.73	1.60	65.60	122.70
4H-4, 78–80	32.58	30.71	32.17	1.49	64.38	123.80
4H-5, 80–82	34.10	29.76	22.53	2.29	54.57	79.11
4H-6, 80–82	35.60	27.71	22.64	1.89	52.24	65.59
5H-1, 85–87	37.65	24.26	25.96	1.83	52.06	78.50
5H-2, 85–87	39.15	23.64	21.78	1.77	47.19	69.66
5H-3, 85–87	40.65	26.15	19.57	1.85	47.58	68.28
5H-4, 85–87	42.15	25.97	19.24	3.02	48.23	36.94
5H-5, 85–87	43.65	20.19	14.74	1.24	36.17	54.76
5H-6, 85–87	45.15	22.91	18.96	1.65	43.52	74.10
6H-1, 85–87	47.25	22.78	16.04	1.08	39.91	53.38
6H-2, 85–87	48.75	22.40	17.44	1.66	41.51	55.96
6H-3, 85–87	50.25	23.04	18.39	2.12	43.54	74.19
6H-4, 85–87	51.75	20.40	17.41	1.76	39.57	35.52
6H-5, 85–87	53.25	20.71	14.38	1.40	36.48	40.38
7H-1, 85–87	56.95	20.57	17.75	3.09	41.42	56.95
7H-2, 85–87	58.45	22.66	22.21	3.69	48.56	91.15
7H-3, 85–87	59.95	31.54	16.44	1.84	49.82	56.20
7H-4, 85–87	61.45	34.20	14.44	1.24	49.88	39.60
7H-5, 85–87	62.95	38.02	12.99	0.81	51.82	96.44
7H-6, 85–87	64.45	28.43	16.87	1.80	47.11	64.43
8H-1, 85–87	66.65	25.37	9.70	0.68	35.75	95.14
8H-2, 85–87	68.15	30.61	16.97	0.94	48.51	85.85
8H-3, 85–87	69.65	28.33	24.19	0.99	53.50	46.42
8H-4, 85–87	71.15	31.17	22.78	1.36	55.31	73.38
8H-5, 85–87	72.65	26.61	25.26	1.22	53.09	38.46
8H-6, 85–87	74.15	25.40	21.21	0.86	47.46	55.50
9H-1, 85–87	76.25	12.90	33.43	16.68	63.00	40.67
9H-2, 85–87	77.75	14.50	12.96	19.77	47.23	16.02
9H-3, 85–87	79.25	22.19	17.02	1.43	40.64	24.22
9H-4, 85–87	80.75	22.65	14.46	1.04	38.15	72.29
9H-5, 85–87	82.25	29.89	15.75	1.35	46.99	47.30
9H-6, 85–87	83.75	27.84	15.87	1.27	44.99	38.48
10H-1, 85–87	85.85	29.81	15.83	1.11	46.75	52.67
10H-3, 85–87	88.85	35.59	20.68	1.76	58.03	66.85
10H-4, 85–87	90.35	34.80	22.06	2.08	58.94	75.57
10H-5, 85–87	91.85	32.32	19.84	2.45	54.61	92.89
10H-6, 85–87	93.40	31.85	30.26	2.02	64.14	88.94
11H-1, 85–87	95.55	26.63	29.41	1.98	58.02	54.17
11H-2, 90–92	97.10	24.05	44.39	3.41	71.84	142.60
11H-3, 85–87	98.55	15.44	59.79	11.67	86.89	110.70
11H-4, 85–87	100.05	15.33	63.19	10.57	89.08	132.80
11H-5, 85–87	101.55	14.06	55.61	13.05	82.72	105.60
11H-5, 135–137	102.05	16.91	38.59	17.59	73.09	57.03

Table 2. Gain-size data from Hole 754A.

Core, section, interval (cm)	Depth (mbsf)	63 μm (wt%)	150 μm (wt%)	425 μm (wt%)	Total coarse fraction (%)	Median grain size (μm)
121-754A-						
1H-1, 78–80	0.78	22.25	30.53	4.40	57.17	80.25
1H-2, 78–80	2.28	37.86	38.58	3.70	80.14	117.10
1H-3, 78–80	3.78	45.66	22.54	2.22	70.43	70.94
1H-4, 78–80	5.28	33.65	27.56	3.45	64.66	67.33
2H-1, 78–80	6.88	35.14	27.46	3.54	66.15	49.19
2H-2, 78–80	8.38	34.72	27.39	1.44	63.56	96.65
2H-3, 78–80	9.88	18.64	19.07	3.27	40.97	52.65
2H-4, 78–80	11.38	24.37	27.02	3.57	54.96	62.63
2H-5, 78–80	12.88	21.97	31.20	4.62	57.79	48.74
2H-6, 78–80	14.38	24.89	29.77	3.30	57.97	92.28
3H-1, 78–80	16.48	27.76	31.26	3.01	62.03	54.34
3H-2, 78–80	17.98	27.89	29.15	2.15	59.19	62.81
3H-3, 78–80	19.48	27.71	30.92	1.87	60.49	55.93
3H-4, 78–80	20.98	31.90	23.32	0.77	55.99	72.19
3H-5, 78–80	22.48	24.60	19.10	2.16	45.86	59.13
3H-6, 78–80	23.98	29.82	21.07	3.24	54.14	50.04
4H-1, 78–80	26.08	38.35	24.11	0.60	63.06	62.29
4H-2, 78–80	27.58	36.74	27.35	1.28	65.37	57.47
4H-3, 78–80	29.08	32.63	24.69	1.04	58.36	63.04
4H-4, 78–80	30.58	29.12	22.86	1.15	53.13	59.55
4H-5, 78–80	32.08	30.66	21.95	1.19	53.79	72.05
4H-6, 78–80	33.58	32.74	19.97	0.83	53.54	89.08
5H-1, 78–80	35.68	37.77	24.42	0.55	62.74	77.32
5H-2, 78–80	37.18	28.11	25.77	0.94	54.82	69.74
5H-3, 78–80	38.68	29.50	23.16	1.58	54.23	54.99
5H-4, 78–80	40.18	30.79	25.01	1.93	57.73	54.63
5H-5, 78–80	41.68	32.50	23.87	1.27	57.64	65.09
5H-6, 78–80	43.18	36.32	22.82	1.65	60.79	79.40
6H-1, 78–80	45.28	28.91	17.92	1.41	48.24	64.13
6H-2, 78–80	46.78	33.25	20.09	0.76	54.09	54.84
6H-3, 78–80	48.28	34.60	17.62	0.63	52.85	71.35
6H-4, 78–80	49.78	24.08	22.27	1.33	47.68	72.65
6H-5, 78–80	51.28	20.72	16.51	1.23	38.46	30.13
6H-6, 78–80	52.78	21.55	18.19	1.15	40.89	42.36
7H-1, 78–80	54.88	18.22	13.51	1.63	33.36	41.44
7H-2, 78–80	56.38	20.18	11.83	1.05	33.06	12.80
7H-3, 78–80	57.88	24.09	15.69	1.22	41.00	20.59
7H-4, 78–80	59.38	20.98	14.80	1.42	37.19	30.31
7H-5, 78–80	60.88	17.72	12.10	0.94	30.75	8.06
7H-6, 78–80	62.38	22.06	14.22	1.32	37.60	39.20
8H-1, 78–80	64.58	20.53	14.26	1.23	36.01	7.89
8H-2, 78–80	66.08	20.56	11.85	1.06	33.47	15.23
8H-3, 78–80	67.58	16.15	11.82	0.95	28.92	13.28
8H-4, 78–80	69.08	17.82	17.23	1.77	36.82	19.95
8H-5, 78–80	70.58	16.62	12.64	1.74	31.00	12.84
8H-6, 78–80	72.08	19.92	16.10	2.02	38.05	22.77
8H-7, 78–80	73.58	20.26	15.49	2.59	38.33	26.63
9H-1, 78–80	74.28	21.78	19.05	2.43	43.26	25.77
9H-2, 78–80	75.78	22.32	16.03	1.83	40.17	13.61
9H-3, 78–80	77.28	24.47	11.46	1.40	37.33	38.97
9H-4, 78–80	78.78	27.67	15.43	0.87	43.97	36.12
9H-5, 78–80	80.28	26.05	16.88	1.51	44.44	18.41
9H-6, 78–80	81.78	30.52	13.15	11.36	55.02	15.22
10H-1, 78–80	83.98	23.37	15.90	0.50	39.76	24.90
10H-2, 78–80	85.48	27.88	20.76	0.97	49.60	64.88
10H-3, 78–80	86.98	24.25	23.05	0.79	48.09	29.93
10H-4, 78–80	88.48	25.20	15.94	0.92	42.05	26.38
10H-5, 78–80	89.98	24.78	10.75	1.92	37.45	9.83
10H-6, 78–80	91.48	25.71	16.93	0.85	43.49	8.97
11H-1, 78–80	93.68	25.92	18.55	1.07	45.55	53.35
11H-2, 78–80	95.18	16.97	10.23	0.97	28.17	9.47
11H-3, 78–80	96.68	20.73	9.60	0.81	31.14	36.89
11H-4, 80–82	98.20	26.44	13.48	1.20	41.12	55.33
11H-5, 78–80	99.68	29.99	16.21	2.05	48.24	46.34
11H-6, 78–80	101.18	31.51	12.79	1.01	45.31	29.07
12H-1, 78–80	103.38	34.78	15.37	1.18	51.33	80.80
12H-2, 78–80	104.88	36.89	16.25	2.36	55.50	66.29
12H-3, 78–80	106.38	39.04	15.59	1.53	56.16	90.02
12H-4, 78–80	107.88	35.10	10.71	2.36	48.17	69.36
12H-5, 78–80	109.38	37.90	12.20	1.56	51.66	43.03
12H-6, 78–80	110.88	35.42	12.17	0.88	48.47	57.05
13H-1, 78–80	113.08	31.06	6.45	0.57	38.08	78.22
13H-2, 78–80	114.58	32.48	9.06	0.93	42.47	56.46
13H-3, 78–80	116.08	37.77	17.73	1.63	57.13	84.02
14H-1, 78–80	122.78	36.11	30.83	5.46	72.40	114.00
14H-2, 78–80	124.28	33.09	33.93	5.91	72.93	106.40
14H-3, 78–80	125.78	24.78	33.36	10.87	69.01	109.20

increases in the lowermost Miocene and Oligocene portions of the records and is coarsest beneath the Oligocene disconformity in the upper Eocene shallow-water deposits which overlie the Eocene angular unconformity on Broken Ridge (Figs. 2 and 3).

Comparisons of these records with the biostratigraphy (Peirce, Weissel et al., 1990) shows that the Pliocene-Pleistocene grain size (upcore) increase occurred in part or all of Zones CN12 and CN13. The grain-size increase in the earlier late Miocene occurred between Zone CN5/CN6, the minimum, and Zone CN7/CN8. The lower Miocene grain-size minimum occurs in Zone CN1.

Oxygen isotope analyses conducted on benthic foraminifers from the same samples used for the grain-size analyses (Rea et al., this volume) permit the winnowing events indicated by the size variations to be placed within the δ18O stratigraphy (Figs. 4 and 5). The δ18O records from Holes 752A and 754A both show the isotopic enrichments known from the early middle Miocene and the upper Pliocene. The mid-Miocene enrichment is about 1.0 per mil and the upper Pliocene enrichment is 0.7 to 0.8 per mil. Paleodepths of the Broken Ridge drill sites constrain these records to be of the Indian Ocean surface water mass. The data show that the late Miocene increase in bulk sediment grain size occurs 20 to 25 m upcore from the early middle Miocene oxygen isotopic enrichment (Figs. 4 and 5).

DISCUSSION

The grain-size records from Holes 752A and 754A are remarkably similar. We interpret this record mainly in terms of current energy, but other factors also influence grain size in carbonate sediments. The most common of these is dissolution, which acts to fragment foraminifers, thereby reducing the relative abundance of the coarser fractions. Although detailed foraminifer-based dissolution indices have not been generated, we believe dissolution to have played only a minor role on Broken Ridge for three reasons. First, the paleodepths of these samples between 0 and 1100 m over the past 30 m.y. places them 2500 to 3000 m above the top of the lysocline during that time period (Prell and Peterson, 1985; Rea and Leinen, 1985). Second, shipboard and ensuing examination of both planktonic and benthic foraminifers at these sites show that the microfossils are well-preserved throughout the sections studied (Peirce, Weissel, et al., 1989; Nomura, this volume; van Eijden and Smit, this volume). No pteropods were reported from the oozes of Sites 752 or 754, so the question of incomplete aragonite dissolution influencing bulk grain size does not arise here. Third, the temporal distribution of hiatuses, most of which represent dissolution pulses, as summarized by Keller and Barron (1987), bears no resemblance to the Broken Ridge grain-size patterns. Patterns of changing sea-level (Haq et al., 1987) also bear no resemblance to the grain-size variations.

The coarse lowermost samples in each hole are late Eocene in age and represent the period of shallow water and significant erosion atop Broken Ridge during its initial post-uplift submergence. Sediments become finer grained above the Oligocene disconformity and reach a minimum in grain size in earliest Miocene time. We interpret this grain-size reduction which spans about 15 m.y. including the lacuna as reflecting the subsidence of Broken Ridge after its mid-Eocene emergence and the lessening effect of surface-water influence (Rea et al., 1990). As subsidence continues, the remaining patterns most likely reflect winnowing.

The uppermost middle Miocene increase in the sediment grain size occurs about 20 m upcore from the shift in oxygen isotopes that signifies the increase in Antarctic ice volume (Figs. 4 and 5). The upper Pliocene grain-size increase is also upcore from the δ18O indication of ice growth, but by only perhaps 8 or 9 m. Using the sedimentation rates calculated by Rea et al. (1990), the Miocene current intensification occurred 2 to 3 m.y. after the ice buildup on Antarctica, and the Pleistocene current intensification
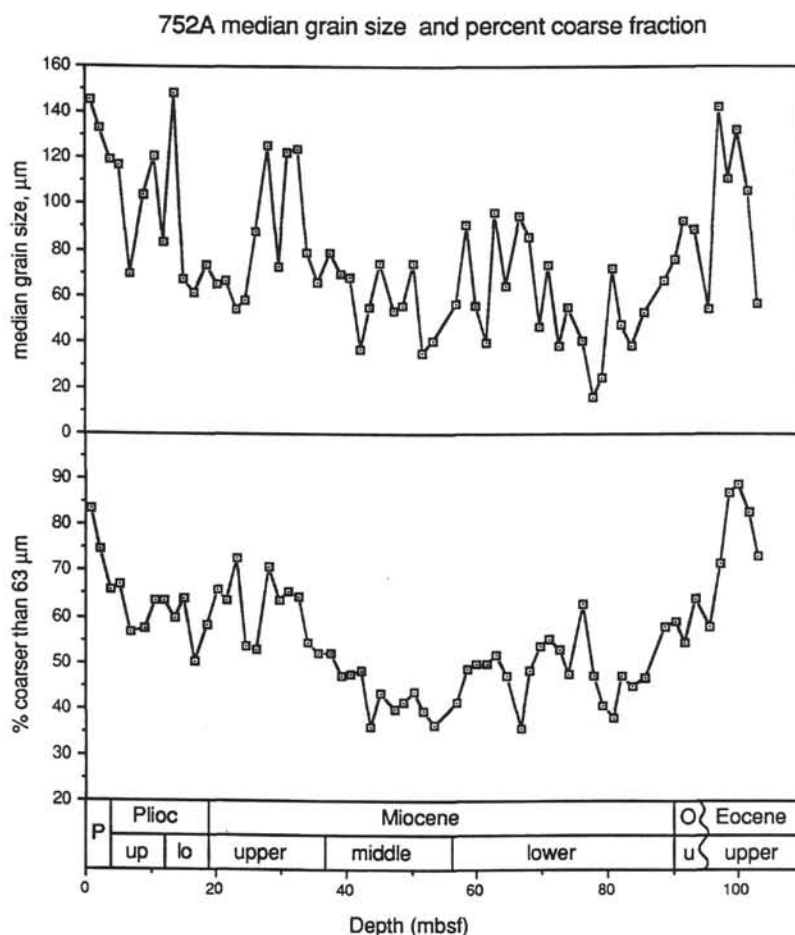
Figure 2. Grain size of bulk sediment at Hole 752A. Median diameter as determined by Coulter Counter (above); weight percent of material coarser than 63 μm (below).

occurred as much as 1 m.y. after the Northern Hemisphere ice volume buildup. This first observation supports the original suggestion of Kennett (1977, 1985) that the Antarctic ice volume increase was not accompanied by important polar cooling, but that the increase in the planetary temperature gradient occurred at the end of the middle Miocene. These data are also consistent with the information presented by Rea and Bloomstine (1985), Leinen (1979), and Miller et al. (1987) that atmospheric and oceanic surface circulation increased about 10 Ma and not at about 13 Ma.

The apparent lag between the isotopic indication of Northern Hemisphere ice buildup and the intensification of Southern Hemisphere sea-surface circulation is consistent with the observation made first by Flohn (1981) that the hemispheres may be somewhat independent in their circulatory behavior; a cooling at one pole and concomitant increase in the temperature gradient of that hemisphere need not serve to increase the circulation energy of the other. Indications of the intensity of Southern Hemisphere atmospheric circulation do not appear to reflect any changes associated with the onset of Northern Hemisphere glaciation (Rea, 1989). Results of this study suggest that the rapid buildup of ice in polar regions, therefore, should not be taken to signify an immediate increase in the energies of atmospheric and sea-surface circulation either on a global or a hemispherical basis.

ACKNOWLEDGMENTS

REFERENCES

Berggren, W. A., Kent, D. V., Flynn, J. J., and Van Couvering, J. A., 1985. Cenozoic geochronology. *Geol. Soc. Am. Bull.*, 96:1407–1418.

Bolli, H. M., Saunders, J. B., and Perch-Nielsen, K. (Eds.), 1985. *Plankton Stratigraphy:* Cambridge (Cambridge Univ. Press).

Davies, T. A., Luyendyk, B. P., et al., 1974. *Init. Repts. DSDP*, 26: Washington (U.S. Govt. Printing Office).

Dowding, L. G., 1977. Sediment dispersal within the Cocos Gap, Panama Basin. *J. Sediment. Petrol.*, 47:1132–1156.

Flohn, H., 1981. A hemispheric circulation asymmetry during late Tertiary. *Geol. Rundsch.*, 70:725–736.

Halfman, J. D., and Johnson, T. C., 1984. Enhanced atmospheric circulation over North America during the early Holocene: evidence from Lake Superior. *Science*, 224:61–63.

Haq, B. U., Hardenbol, J., and Vail, P. R., 1987. Chronology of fluctuating sea levels since the Triassic. *Science*, 235:1156–1167.

Keller, G., and Barron, J. A., 1987. Paleodepth distribution of Neogene deep-sea hiatuses. *Paleoceanography*, 2:697–713.

Kennett, J. P., 1977. Cenozoic evolution of Antarctic glaciation, the circum-Antarctic Ocean, and their impact on global paleoceanography. *J. Geophys. Res.*, 82:3843–3860.

_____, 1986. Miocene to early Pliocene oxygen and carbon isotope stratigraphy of the Southwest Pacific, DSDP Leg 90. *In* Kennett, J. P., von der Borch, C. C., et al., *Init. Repts. DSDP*, 90 (Pt. 2): Washington (U.S. Govt. Printing Office), 1383–1411.

Kowsmann, R. O., 1973. Coarse components in surface sediments of the Panama Basin, eastern Equatorial Pacific. *J. Geol.*, 81:473–494.

Ledbetter, M. T., 1981. Paleooceanographic significance of bottom-current fluctuations in the Southern Ocean. *Nature*, 294:554–556.

_____, 1986. Bottom-current pathways in the Argentine Basin revealed by mean silt particle size. *Nature*, 321:423–425.

Ledbetter, M. T., and Johnson, D. A., 1976. Increased transport of Antarctic Bottom Water in the Vema channel during the last ice age. *Science*, 194:837–839.

Leinen, M., 1979. Biogenic silica accumulation in the central equatorial Pacific and its implications for Cenozoic paleoceanography. *Geol. Soc. Am. Bull.*, 90 (Pt. 2):1310–1376.

Matthews, R. K., and Poore, R. Z., 1980. Tertiary $\delta^{18}O$ record and glacio-eustatic sea-level fluctuations. *Geology*, 8:501–504.

Miller, K. G., Fairbanks, R. G., and Mountain, G. S., 1987. Tertiary oxygen isotope synthesis, sea-level history, and continental margin erosion. *Paleoceanography*, 2:1–19.

Moore, T. C., Jr., Heath, G. R., and Kowsmann, R. O., 1973. Biogenic sediments of the Panama Basin. *J. Geol.*, 81:458–472.

Moore, T. C., Jr., Rabinowitz, P. D., Borella, P. E., Shackleton, N. J., and Boersma, A., 1984. History of the Walvis Ridge. *In* Moore, T. C., Rabinowitz, P. D., et al., *Init. Rept. DSDP*, 74: Washington (U.S. Govt. Printing Office), 873–894.

Peirce, J., Weissel, J.,. et al., 1989. *Proc. ODP, Init. Repts.*, 121: College Station, TX (Ocean Drilling Program).

Peterson, L. C., and Prell, W. L., 1985. Carbonate preservation and rates of climatic change: an 800 kyr record from the Indian Ocean. *In* Sundquist, E. T., and Broecker, W. S. (Eds.), *The Carbon Cycle and Atmospheric CO2*: Natural Variations Archean to Present: Am. Geophys. Union Monogr., 32:251–270.

Prell, W. L., 1977. Winnowing of Recent and late Quaternary deep-sea sediments: Colombia Basin, Caribbean Sea. *J. Sediment. Petrol.*, 47:1583–1592.

Rea, D. K., 1989. Geologic record of atmospheric circulation on tectonic timescales. *In* Leinen, M., and Sarnthein, M. (Eds.), *Paleoclimatology and Paleometeorology: Modem and Past Patterns of Global Atmospheric Transport*: Dordrecht (Klewer Academic Publ.), 841–857.

Rea, D. K., and Bloomstine, M. K., 1986. Neogene history of the South Pacific tradewinds: evidence for hemispherical asymmetry of atmospheric circulation. *Palaeogeogr., Palaeoclimatol., Palaeoecol.*, 55:55–64.

Rea, D. K., Dehn, J., Driscoll, N., Farrell, J., Janecek, T., Owen, R. M., Pospichal, J. L., Resiwati, P., and the ODP Leg 121 Scientific Party, 1990. Paleoceanography of the eastern Indian Ocean from ODP Leg 121 drilling on Broken Ridge. *Geol. Soc. Am. Bull.*, 102:679–690.

Rea, D. K., and Janecek, T. R., 1986. Grain size changes in reworked pelagic sediments, Deep Sea Drilling Project Site 599. *In* Leinen, M., Rea, D. K., et al., *Init. Repts. DSDP*, 92: Washington (U.S. Govt. Printing Office), 341–343.

Rea, D. K., and Leinen, M., 1985. Neogene history of the calcite compensation depth and lysocline in the South Pacific Ocean. *Nature*, 316:805–807.

Rea, D. K., Leinen, M., and Janecek, T. R., 1985. Geologic approach to the long-term history of atmospheric circulation. *Science*, 227:721–725.

Savin, S. M., Douglas, R. G., and Stehli, F. G., 1975. Tertiary marine paleotemperatures. *Geol. Soc. Am. Bull.*, 86:1499–1510.

Shackleton, N. J., Moore, T. C., Jr., Rabinowitz, P. D., Boersma, A., Borella, P. E., Chave, A. D., Duee, G., Futterer, D., Jiang, M.-J., Kleinert, K., Lever, A., Manivit, H., O'Connell, S., and Richardson, S. H., 1984. Accumulation rates in Leg 74 sediments. *In* Moore, T. C., Jr., Rabinowitz, P. D., et al., *Init. Repts DSDP*, 74: Washington (U.S. Govt. Printing Office), 621–637.

van Andel, T. H., 1973. Texture and dispersal of sediments in the Panama Basin. *J. Geol.*, 81:434–457.

_____, 1975. Mesozoic/Cenozoic calcite compensation depth and the global distribution of calcareous sediments. *Earth Planet. Sci. Lett.*, 26:187–194.

van Andel, T. H., Thiede, J., Sclater, J. G., and Hay, W. W., 1977. Depositional history of the South Atlantic Ocean during the last 125 million years. *J. Geol.*, 85:651–698.

Woodruff, F., Savin, S. M., and Douglas, R. G., 1981. Miocene stable isotope record: a detailed deep Pacific Ocean study and its paleoclimatic implications. *Science*, 212:665–668.

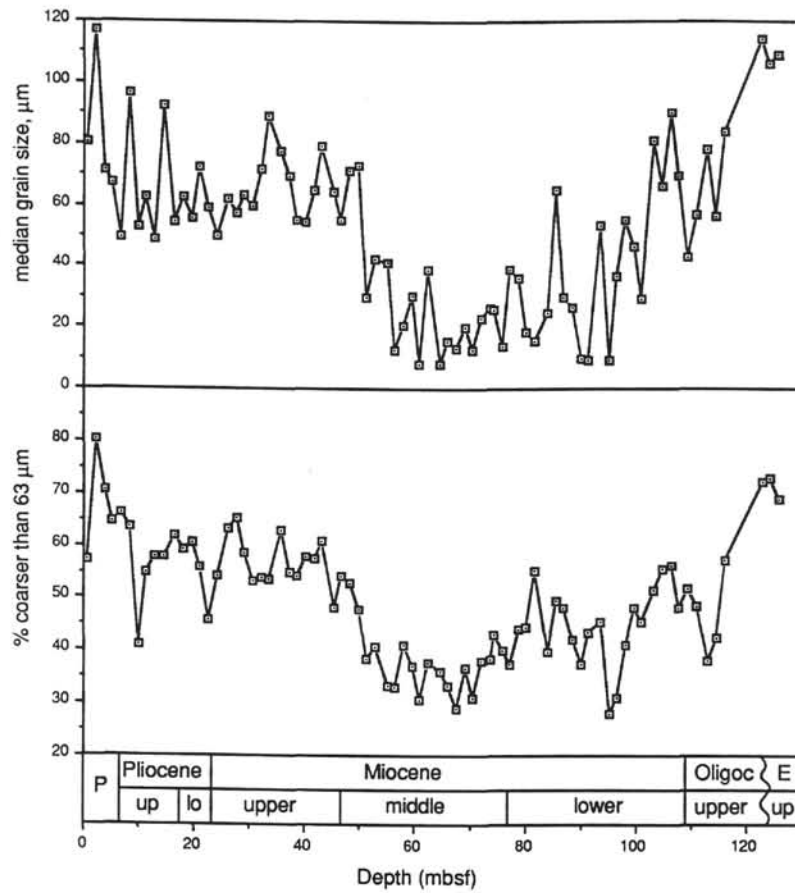754A median grain size and percent coarse fraction

Figure 3. Grain size of bulk sediment at Hole 754A. Median diameter as determined by Coulter Counter (above); weight percent of material coarser than 63 μm (below).

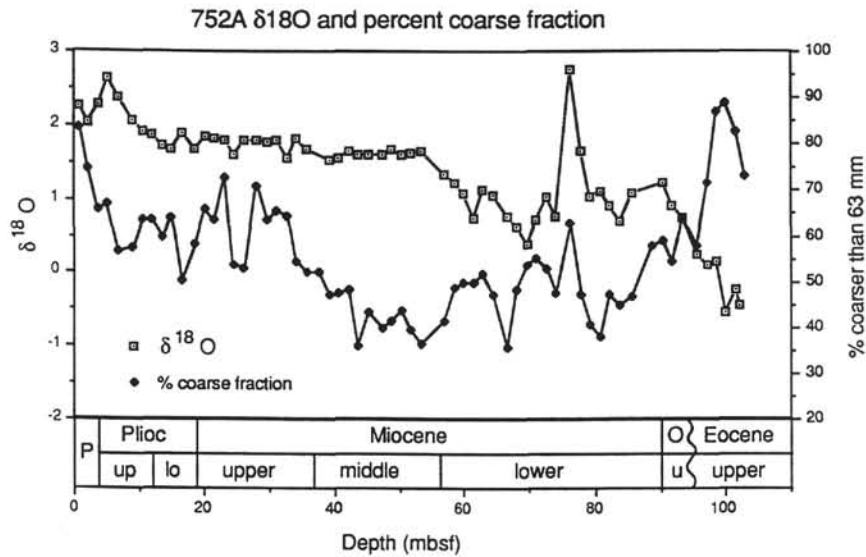752A δ18O and percent coarse fraction

Figure 4. Comparison of the total coarse material and δ18O values of benthic foraminifers for the pelagic oozes of Hole 752A.
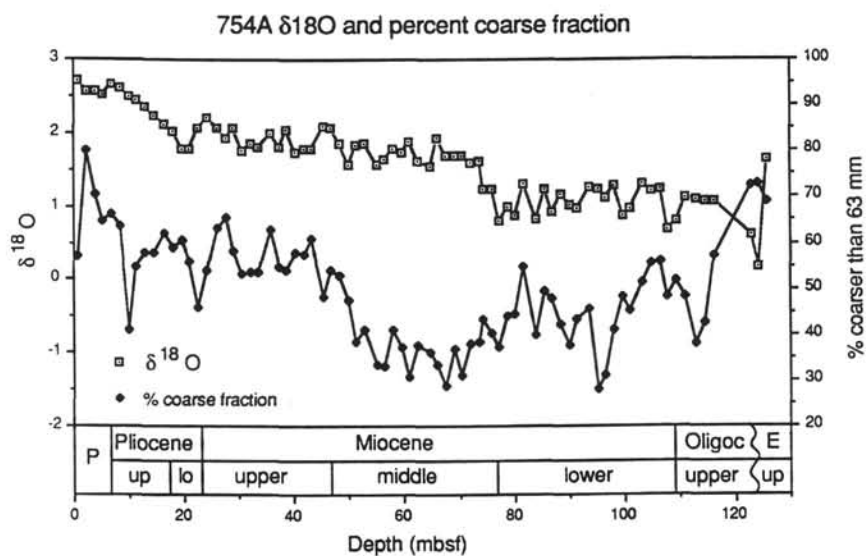
754A δ18O and percent coarse fraction

Figure 5. Comparison of the total coarse material and δ18O values of benthic foraminifers for the pelagic oozes of Hole 754A.